Supporting Information

Regulation of Heteroatom Positioning in Multiple Resonance Thermally Activated Delayed Fluorescence Materials: Performance Optimization for Blue/Red Emission

Lifang Yin,[a] Yi Zhao,[a] Qiang Gao,[a] Yajun Yin,[a] Tengfei He,[a] Yufei Yang,[a] Aimin Ren,[a] Tongshun Wu,[b] Hui Li,[a] Luyi Zou*,[a]

[a] Institute of Theoretical Chemistry, College of Chemistry, Jilin University, Changchun 130023, P. R. China

[b] Key Laboratory of Functional Materials Physics and Chemistry of Ministry of Education, Jilin Normal University, Changchun 130103, China

*Corresponding author: zouly@jlu.edu.cn.

Content

Figures and Tables

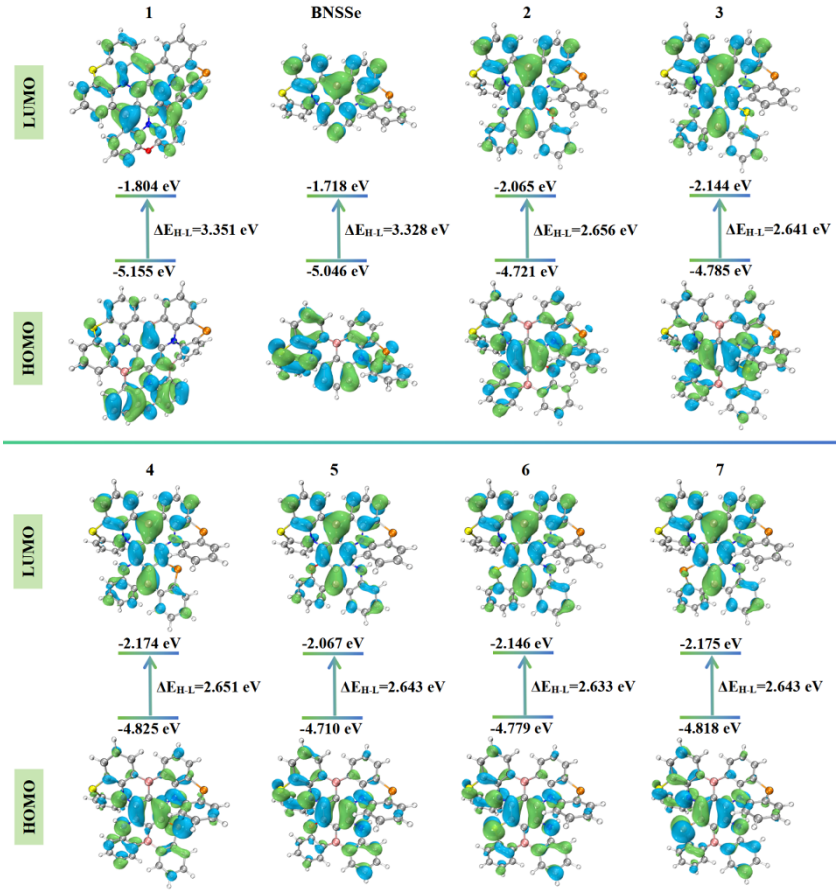

Fig. S1 The energy levels of HOMO and LUMO, $\Delta E_{H\text{-}L}$, ΔE_{ST}, and their orbital distributions in the S_0 state of the investigated molecules.

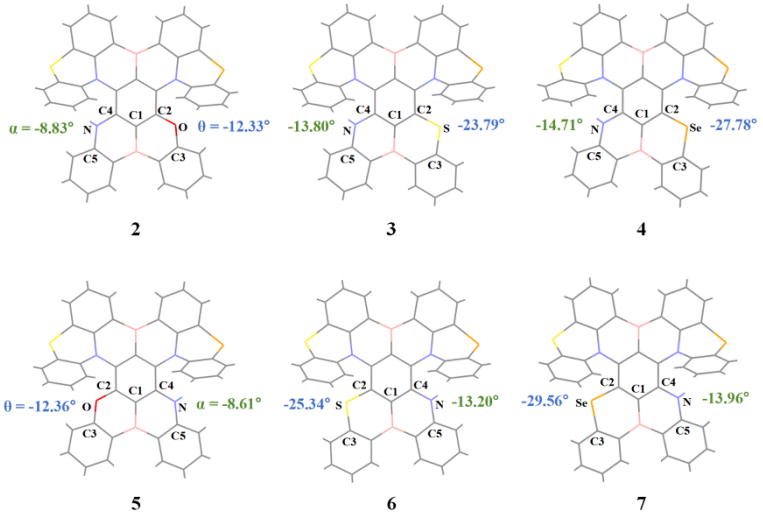

Fig. S2 Geometric structures of S_1 state and key dihedral angles θ (C_1-C_2-X-C_3) and α (C_1-C_4-N-C_5) parameters of the investigated red emitters.

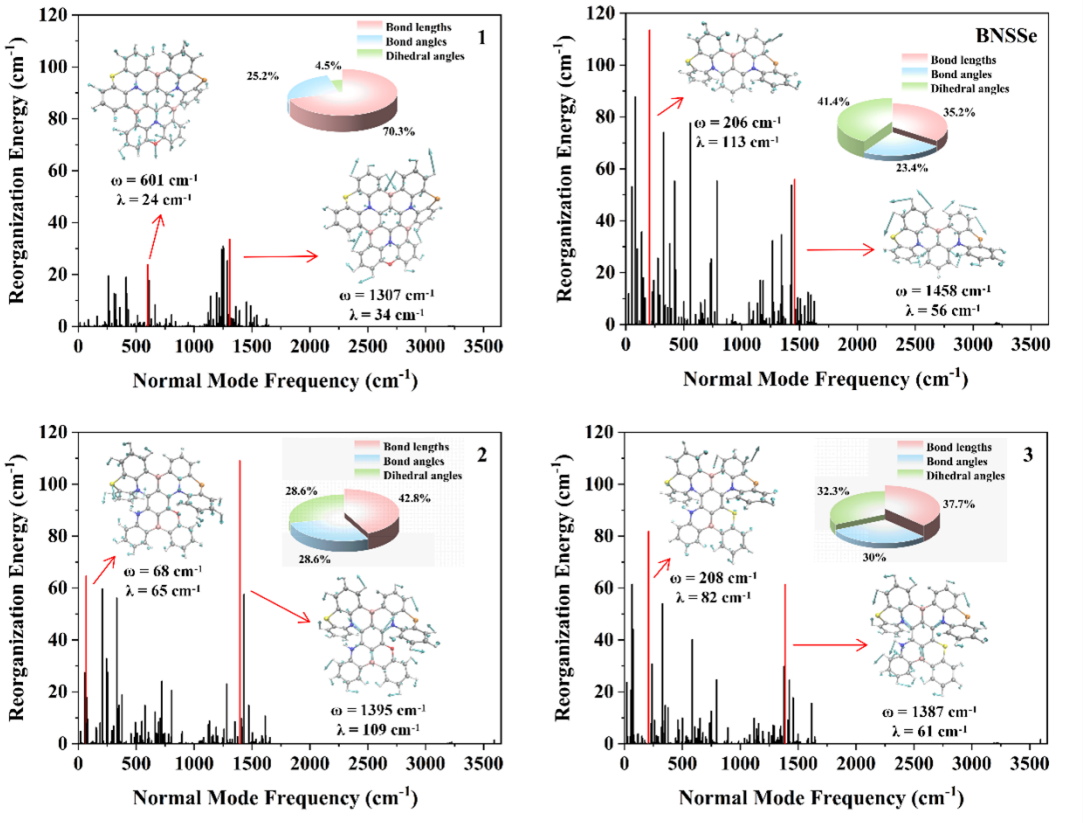

Fig. S3 Calculated reorganization energy for investigated molecules **BNSSe** and **1**–**3** between the S_1 and S_0 states. Inset: Shift vectors for the normal modes have the largest reorganization energies in the low and high frequency regions, as well as the contributions of bond lengths, bond angles, and dihedral angles to the reorganization energy.

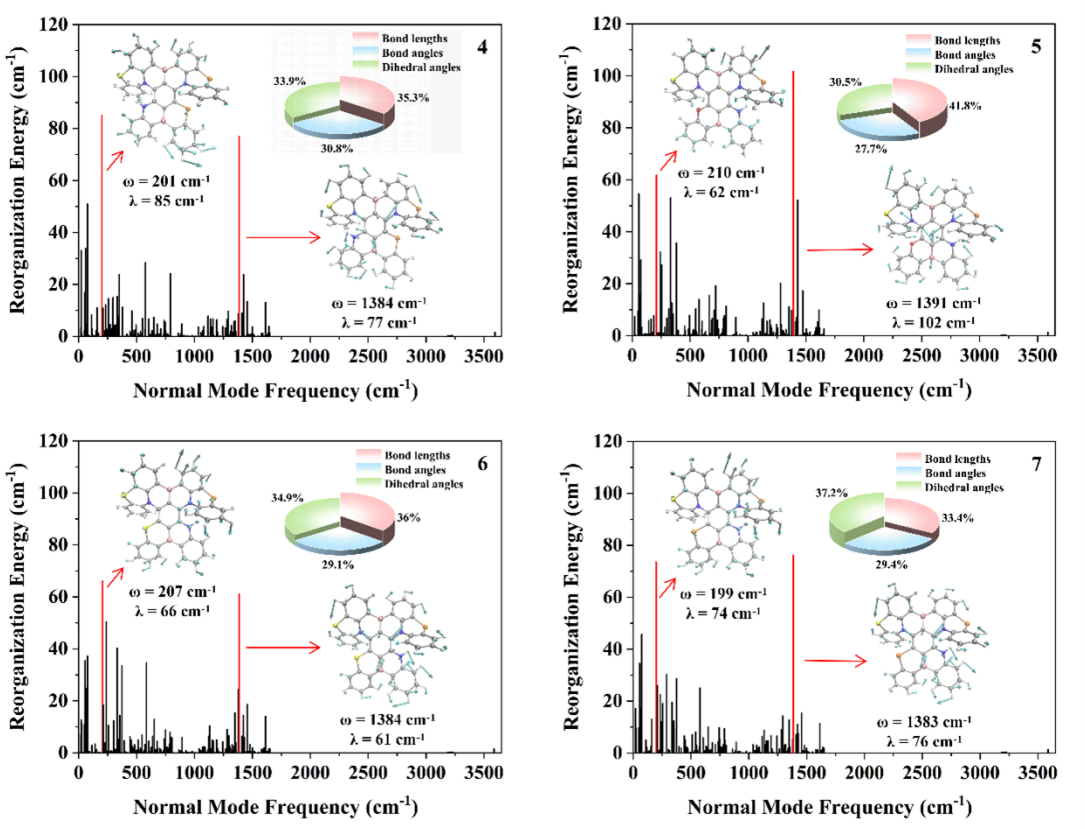

Fig. S4 Calculated reorganization energy for investigated molecules **4**–**7** between the S_1 and S_0 states. Inset: Shift vectors for the normal modes have the largest reorganization energies in the low and high frequency regions, as well as the contributions of bond lengths, bond angles, and dihedral angles to the reorganization energy.

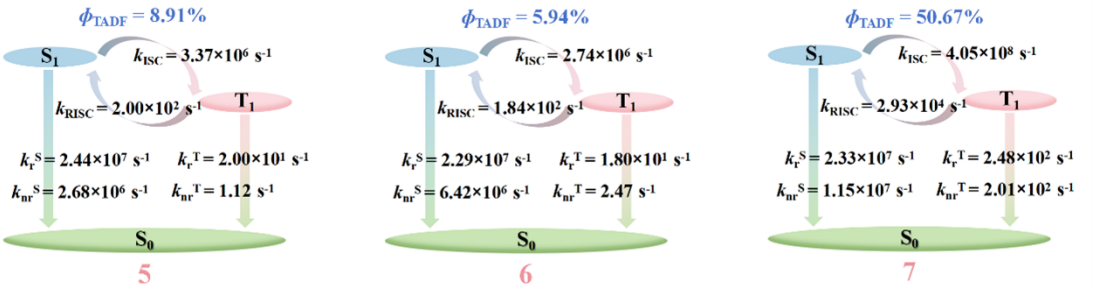

Fig. S5 Relevant transition rates and ϕ_{TADF} at room temperature for the investigated molecules **5**–**7**.

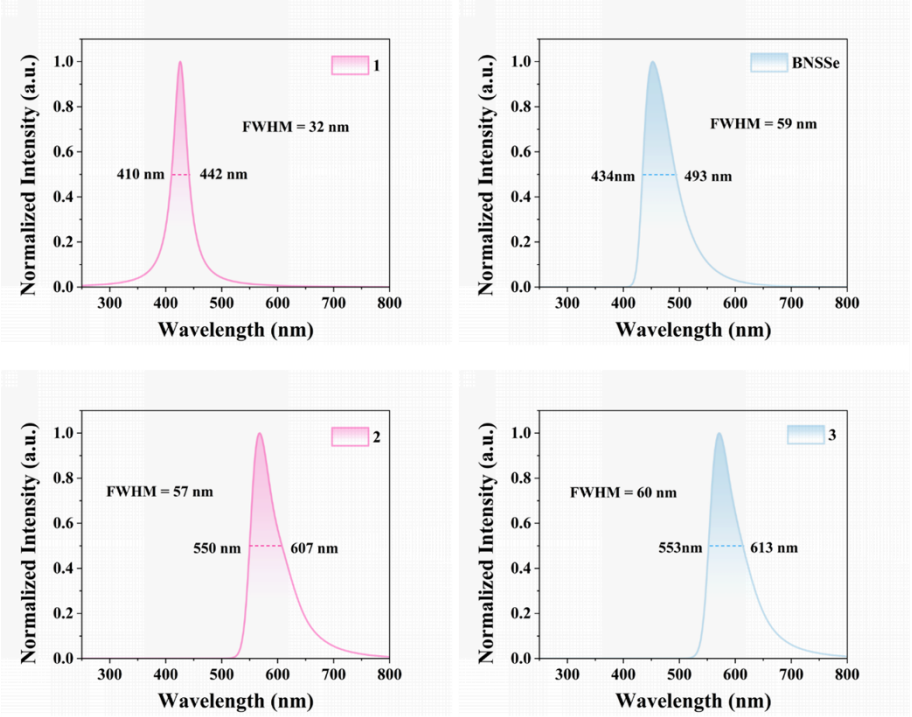

Fig. S6 Vibrationally resolved emission spectra and FWHM (nm) of the investigated molecules **BNSSe** and **1**–**3**.

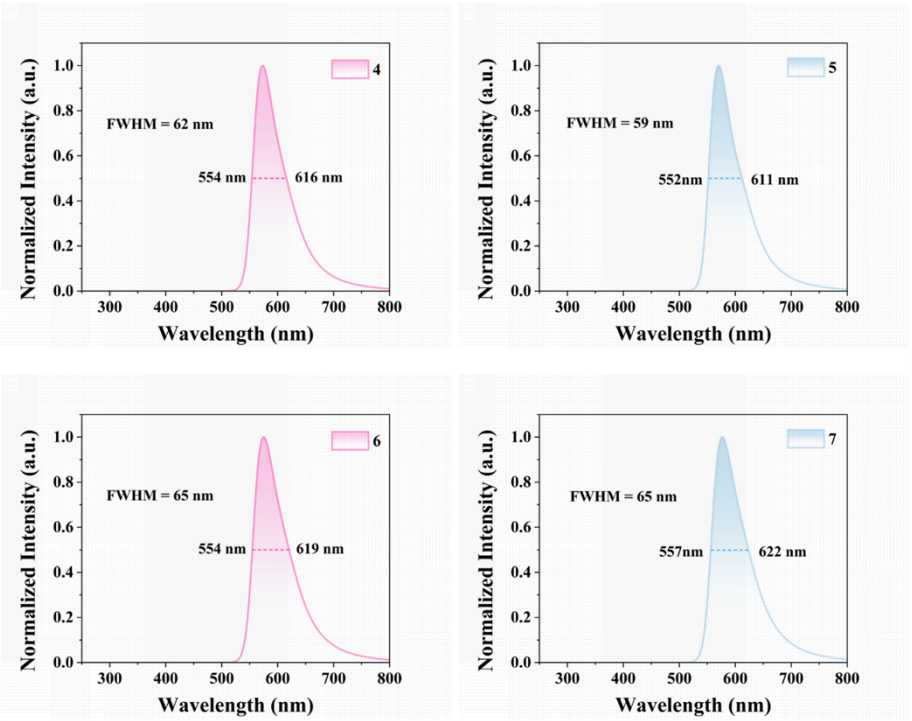

Fig. S7 Vibrationally resolved emission spectra and FWHM (nm) of the investigated molecules **4**–**7**.

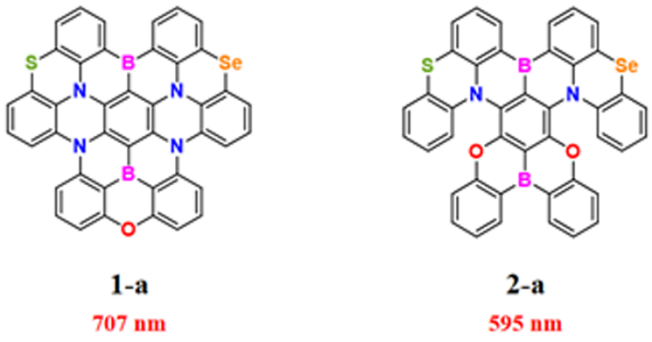

Fig. S8 Schematic diagrams of the structures of the investigated molecules **1-a** and **2-a**.

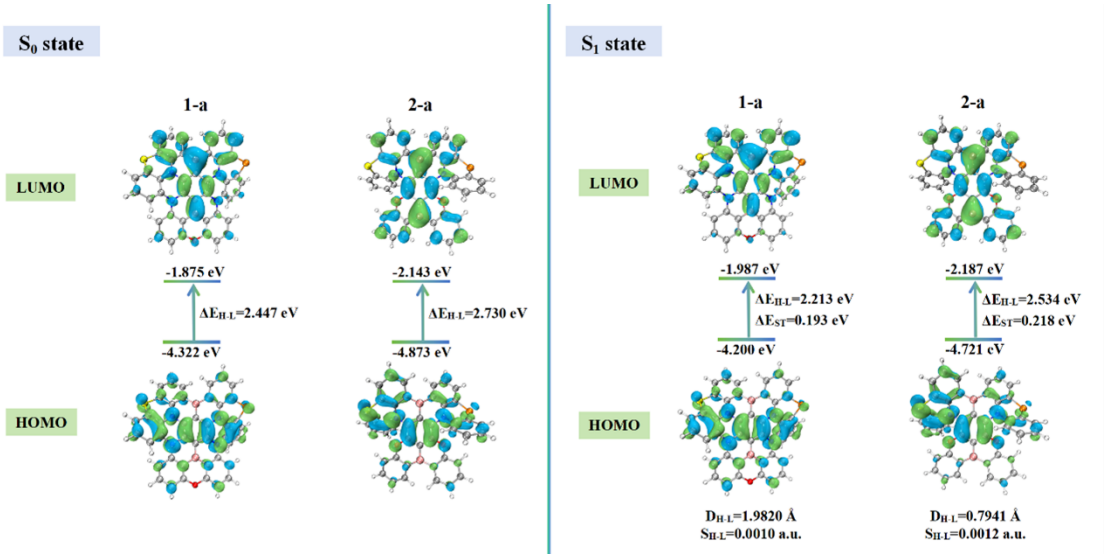

Fig. S9 The energy levels of HOMO and LUMO, $\Delta E_{H\text{-}L}$, ΔE_{ST}, and their orbital distributions in the S_0/S_1 state of the investigated molecules **1-a** and **2-a**, as well as the $D_{H\text{-}L}$ and $S_{H\text{-}L}$ between HOMO and LUMO in the S_1 state.

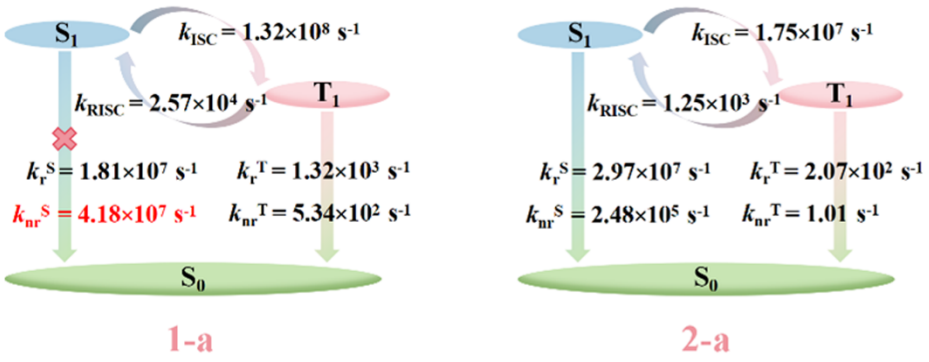

Fig. S10 Relevant transition rates at room temperature for the investigated molecules **1-a** and **2-a**.

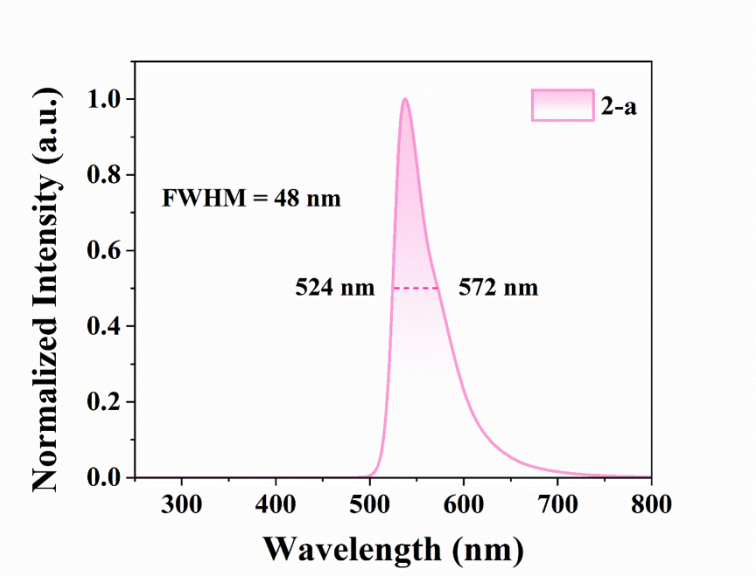

Fig. S11 Vibrationally resolved emission spectra and FWHM (nm) of the investigated molecules **2-a**.

Table S1 Energy levels of **BNSSe** calculated by different methods, along with the corresponding experimental values

BNSSe	E_{S1} (eV)	E_{T1} (eV)	ΔE_{ST} (eV)
B3LYP-D3(BJ)/6-31G(d)	2.459	2.101	0.358
SCS-CC2/cc-pVTZ	2.710	2.607	0.103
Exp.[a]	2.560	2.440	0.120

[a] Experimental values from ref 18

Table S2 ΔE (a.u.), $|\mu|^2$ (a.u.), and f for the $S_1 \rightarrow S_0$ transition of the investigated molecules

	$\Delta E_{(S1\rightarrow S0)}$	$\lvert\mu\rvert^2_{(S1\rightarrow S0)}$	$f_{(S1\rightarrow S0)}$
1	0.0972	1.1043	0.0716
BNSSe	0.0904	2.6009	0.1567
2	0.0726	2.6088	0.1263
3	0.0722	2.4817	0.1195
4	0.0727	2.4965	0.1209
5	0.0721	2.6305	0.1264
6	0.0718	2.4929	0.1194
7	0.0722	2.4958	0.1201

Table S3 Several representative high-efficiency red-emitting MR-TADF molecules

System	λ (nm)	FWHM (nm)	k_r^S (s^{-1})	k_{ISC} (s^{-1})	k_{RISC} (s^{-1})	Ref.
4	627	37	2.37×10^7	5.62×10^8	3.92×10^4	**This Work**
7	631	40	2.33×10^7	4.05×10^8	2.93×10^4	
FSBN	630	59	7.11×10^7	7.40×10^6	1.86×10^4	*Angew. Chem. Int. Ed.* **2025**, 64, e202420253.[1]
Δ-DABNA-TB	613	31	3.10×10^7	9.60×10^6	8.50×10^2	*J. Am. Chem. Soc.* **2024**, 146, 18331−18340.[2]
PPZ-BN	613	48	1.20×10^8	1.40×10^7	2.20×10^4	*Angew. Chem. Int. Ed.* **2023**, 62, e202300934.[3]
BNNO	637	32	7.30×10^7	-	1.40×10^4	*Adv. Mater.* **2023**, 35, 2301018.[4]
BN-R	620	49	3.80×10^7	1.33×10^7	1.13×10^4	*Angew. Chem. Int. Ed.* **2023**, 62, e202216473.[5]
BNO1	610	35	7.40×10^7	-	-	*Adv. Mater.* **2022**, 34, 2201442.[6]
BNO2	618	37	6.10×10^7	-	-	
BNO3	624	38	6.30×10^7	-	-	
R-BN	662	38	7.50×10^7	8.30×10^6	6.70×10^4	Ref.21
R-TBN	692	38	6.20×10^7	8.50×10^6	2.50×10^4	
BBCz-R	619	27	1.30×10^8	-	1.20×10^4	*J. Am. Chem. Soc.* **2020**, 142, 19468−19472.[7]

Table S4 k_r^S, k_{ISC}, k_{RISC}, and FOM (s^{-1}) of molecule **1** and **BNSSe**

	k_r^S	k_{ISC}	k_{RISC}	FOM
1	2.58×10^7	1.74×10^9	1.80×10^8	2.64×10^6
BNSSe	4.99×10^7	2.85×10^7	1.77×10^5	1.34×10^5

Table S5 Vertical excitation energy (eV), oscillator strengths (f), k_r^T (s^{-1}), and lifetimes (τ, μs) of the investigated molecules in $T_1\rightarrow S_0$

	vertical excitation energy	oscillator strengths	k_r^T	τ
1				
T_1^I	2.855	4.10×10^{-8}	1.45×10^1	
T_1^{II}	2.855	2.80×10^{-8}	9.89	
T_1^{III}	2.855	1.39×10^{-5}	4.91×10^3	
$T_{1,av}$			1.65×10^3	607
BNSSe				
T_1^I	2.607	1.43×10^{-6}	4.21×10^2	

T_1^{II}	2.607	3.60×10^{-8}	1.06×10^{1}	
T_1^{III}	2.607	3.70×10^{-8}	1.09×10^{1}	
$T_{1,av}$			1.47×10^{2}	6780
2				
T_1^{I}	1.897	3.09×10^{-7}	4.82×10^{1}	
T_1^{II}	1.897	0.00	0.00	
T_1^{III}	1.897	4.00×10^{-9}	6.24×10^{-1}	
$T_{1,av}$			1.63×10^{1}	61400
3				
T_1^{I}	1.893	1.30×10^{-7}	2.02×10^{1}	
T_1^{II}	1.893	6.80×10^{-8}	1.06×10^{1}	
T_1^{III}	1.893	7.50×10^{-8}	1.17×10^{1}	
$T_{1,av}$			1.41×10^{1}	70700
4				
T_1^{I}	1.907	1.53×10^{-5}	2.42×10^{3}	
T_1^{II}	1.907	1.33×10^{-6}	2.09×10^{2}	
T_1^{III}	1.907	2.97×10^{-5}	4.68×10^{3}	
$T_{1,av}$			2.44×10^{3}	411
5				
T_1^{I}	1.889	3.42×10^{-7}	5.29×10^{1}	
T_1^{II}	1.889	3.90×10^{-8}	6.03	
T_1^{III}	1.889	6.00×10^{-9}	9.28×10^{-1}	
$T_{1,av}$			2.00×10^{1}	50100
6				
T_1^{I}	1.885	7.90×10^{-8}	1.22×10^{1}	
T_1^{II}	1.885	5.00×10^{-8}	7.70	
T_1^{III}	1.885	2.22×10^{-7}	3.42×10^{1}	
$T_{1,av}$			1.80×10^{1}	55500
7				
T_1^{I}	1.897	7.87×10^{-7}	1.23×10^{2}	
T_1^{II}	1.897	2.34×10^{-7}	3.65×10^{1}	
T_1^{III}	1.897	3.74×10^{-6}	5.84×10^{2}	
$T_{1,av}$			2.48×10^{2}	4030

Table S6 Energy difference (eV), SOC (cm^{-1}) and k_{nr}^{T} (s^{-1}) of the investigated molecules in $T_1\rightarrow S_0$

	$E(T_1)–E(S_0)$	$SOC(S_0–T_1)$	k_{nr}^{T}
1	3.028	28.74	3.96×10^{2}
BNSSe	2.873	7.04	2.64×10^{1}
2	2.129	1.40	1.89
3	2.120	0.86	7.27×10^{-1}
4	2.136	12.17	1.43×10^{2}

5	2.121	1.07	1.12
6	2.114	1.58	2.47
7	2.130	14.41	2.01×10^{2}

Table S7 FWHM (nm) of the investigated molecules predicted by the SOGCN model, along with the corresponding experimental value

	1	**BNSSe**	**2**	**3**	**4**	**5**	**6**	**7**
FWHM	40	56/50[a]	42	41	37	42	44	40

[a] Experimental value from ref 18

Table S8 ΔE (eV), λ (cm^{-1}), and k_{nr}^{S} (s^{-1}) between the S_1 and S_0 states of the investigated molecules **BNSSe**,**1-a** and **2-a**

	ΔE	λ_1	λ_2	k_{nr}^{S}
BNSSe	2.974	1632	1303	8.65×10^{6}
1-a	2.151	1116	1081	4.18×10^{7}
2-a	2.445	816	770	2.48×10^{5}

Solid-phase simulation of the BNSSe

Based on the single crystal structure provided in the experimental literature, we optimized the solid-phase structure of **BNSSe** and calculated the non-radiative transition rate (k_{nr}^{S}). We adopted the QM/MM method that combines quantum mechanics (QM) and molecular mechanics (MM), and constructed a 3×3×3 double-layer model using the ONIOM model (Fig. S12).[8] Similarly, the B3LYP-D3(BJ) functional was used as the QM method for calculating the central high-layer molecules; the symmetrically surrounding outer-layer molecules were treated with the Universal Force Field (UFF), which is widely used in MM methods.

The calculated non-radiative transition rate of **BNSSe** in the solid phase is 3.85×10^{6} s^{-1}, which is closer to the experimental value than the calculated value in the gas phase. However, since the simulation is performed on a pure **BNSSe** film, there is still a certain gap compared with the actual doped film with DMIC-TRZ as the host.

Although the solid-phase structure optimized by the QM/MM method and ONIOM model is more consistent with the experimental environment, limited by the lack of single crystal structure data for designed molecules **1**–**7,** we cannot perform the same solid-phase rate calculation. To avoid

the loss of reference significance in the rate comparison of the series of molecules due to inconsistent calculation methods, we ultimately chose to uniformly adopt the gas-phase optimized structure for all molecules. Considering that MR-TADF molecules themselves have high structural rigidity, the simulation deviation of the gas-phase optimized structure from the solid-phase thin film is within an acceptable range, and this method has been verified in many high-level literatures.[1,9]

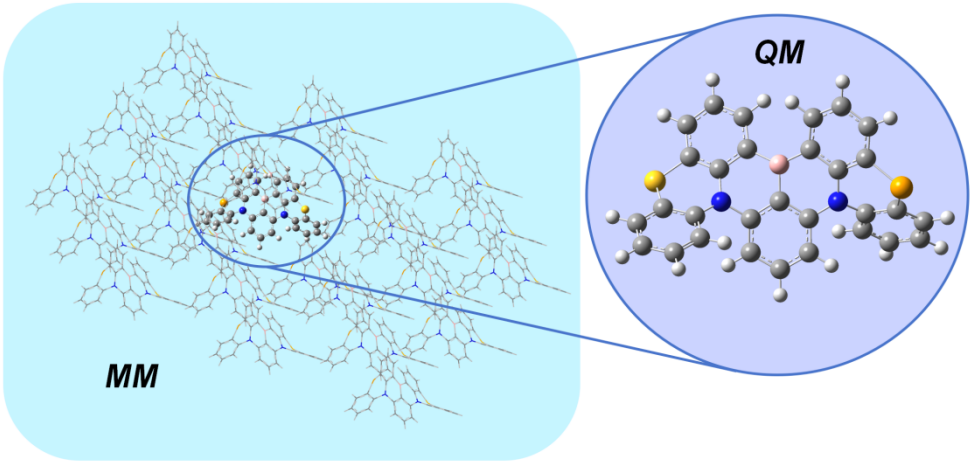

Fig. S12 Schematic diagram of the ONIOM model for the **BNSSe**.

Table S9 Simulations of the non-radiative transition rate (k_{nr}^{S} , s^{-1}) of the **BNSSe** in the gas and solid phases, and the experimental value

BNSSe	gas	solid	exp
(k_{nr}^{S} , s^{-1})	8.65×10^{6}	3.85×10^{6}	0.43×10^{6}

References

S1 Y. Pu, X. Cai, Y. Qu, W. Cui, L. Li, C. Li, Y. Zhang and Y. Wang, *Angew. Chem. Int. Ed.*, 2025, **64**, e202420253.

S2 M. Hayakawa, X. Tang, Y. Ueda, H. Eguchi, M. Kondo, S. Oda, X.-C. Fan, G. N. Iswara Lestanto, C. Adachi and T. Hatakeyama, *J. Am. Chem. Soc.*, 2024, **146**, 18331-18340.

S3 H. Chen, T. Fan, G. Zhao, D. Zhang, G. Li, W. Jiang, L. Duan and Y. Zhang, *Angew. Chem. Int. Ed.*, 2023, **62**, e202300934.

S4 T. Fan, M. Du, X. Jia, L. Wang, Z. Yin, Y. Shu, Y. Zhang, J. Wei, D. Zhang and L. Duan, *Adv. Mater.*, 2023, **35**, 2301018.

S5 X. Cai, Y. Xu, Y. Pan, L. Li, Y. Pu, X. Zhuang, C. Li and Y. Wang, *Angew. Chem. Int. Ed.*, 2023, **62**, e202216473.

S6 Y. Zou, J. Hu, M. Yu, J. Miao, Z. Xie, Y. Qiu, X. Cao and C. Yang, *Adv. Mater.*, 2022, **34**, 2201442.

S7 M. Yang, I. S. Park and T. Yasuda, *J. Am. Chem. Soc.*, 2020, **142**, 19468-19472.

S8 T.-F. He, A.-M. Ren, G.-H. Li, Z.-X. Qu, J.-F. Guo, X.-L. Hao, Y.-N. Chen, L. Shen, Y.-L. Zhang and L.-Y. Zou, *J. Phys. Chem. Lett.*, 2021, **12**, 2232-2244.

S9 K. Shizu and H. Kaji, *Nat. Commun.*, 2024, **15**, 4723.